LIDS-P-1441 March 1985

Tomographic Methods for Multidimensional Born Inversion with a Wide-Band Source*

Cengiz Esmersoy**
Bernard C. Levy†

*Submitted for presentation at the Society of Exploration Geophysicists annual meeting in Washington, D.C. in Oct. 1985. This research was supported in part by the Army Research Office under Grant No. DAAG29-84-K-0005.

**Earth Resources Laboratory Department of Earth, Atmospheric and Planetary Sciences, Massachusetts Institute of Technology, Cambridge, MA. 02139

†Department of Electrical Engineering and Computer Science, Massachusetts Institute of Technology, Cambridge, MA. 02139

Tomographic Methods for Multidimensional Born Inversion with a Wide-Band Source

Cengiz Esmersoy, *Department of Electrical Engineering and Computer Science and Earth Resources Laboratory Department of Earth, Atmospheric and Planetary Sciences Massachusetts Institute of Technology, Cambridge, Massachusetts 02139*

Bernard C. Levy, *Department of Electrical Engineering and Computer Science Massachusetts Institute of Technology, Cambridge, Massachusetts 02139*

Abstract

Two methods for inverting the velocities of a multidimensional acoustic medium within the homogeneous Born approximation are presented. In both methods, the data is obtained by using a wide band source and an array of receivers. The transmitted waves as well as the reflected waves are utilized for inversion. In the first method the medium is excited by a single point source and the scattered field is observed all around the medium. In the second method the medium is probed by a single plane wave (in some cases this can be viewed as the far field of a point source) and the scattered field is observed along a line receiver array. It is shown that, in both cases, the direct inversion problem can be reduced to a straight line tomography problem. In the first method this is done by backpropagating the filtered and time-reversed traces into the medium and imaging the field at time zero. This zero time image provides the projections of the velocity function for all projection angles. Velocities are, then, obtained by the inverse Radon transform. In the case of a plane wave source, it is shown that the slant-stack (Radon transform) of the observed traces along the receiver line is directly related to one projection of the velocity function. Different slant-stack slopes provide projections at different angles. For a single line receiver array, the projection angles cover a range of ninety degrees. The velocites can, therefore, be reconstructed partially in this case. For a complete set of projections either two receiver arrays on both sides of the medium, or two pane waves incident from opposite directions are required.

Introduction

Direct inversion of the velocities of an acoustic medium within the Born approximation has been an active research topic in recent years. Most solutions for the multidimensional case assume an observation geometry consisting of source and receiver arrays. Cohen and Bleistein, 1979, describe a homogeneous background Born inversion method for zero-offset (CDP stack) reflection data. Raz, 1981, considers the before stack data for the same experiment. Clayton and Stolt, 1981, present a Born-WKBJ method to recover density and bulk modulus from reflection data. A slightly different approach to the direct inversion problem has been developed by extending x-ray tomographic techniques to ultrasonic imaging (Wolf, 1969, Mueller et. al., 1979 and Devaney, 1984). In this case, the medium is probed by monochromatic plane waves incident from various directions. These methods use the transmitted waves as well as the reflected waves.

In this paper we present two methods that reduce the Born velocity inversion problem to a straight line tomography problem. It is shown that projections of the velocity function

$$\gamma(\underline{r}) = \frac{c^2}{v^2(\underline{r})} - 1 , \qquad (1)$$

at various projection angles can be obtained from the observed traces. Here, $\underline{r} = (x,z)$ is the spatial coordinates, $v(\underline{r})$ is the medium velocity and $c = \omega/k$ is the background velocity. In the first method the medium is excited by a singe wide-band point source and receivers are located all around the medium. Therefore, the whole scattered field is used in the inversion. A complete set of projections is obtained from the observed traces. In the second method the medium is excited by a plane wave and the scattered field is observed along a line array of receivers. Depending on the incidence angle of the plane wave, the observed data contains both reflected and transmitted waves, in varying proportion. As will be seen in the following, projections of the velocity function at angles $\vartheta_s/2 \le \varphi \le (\vartheta_s - \pi)/2$ are obtained for a single receiver array and a plane wave with incidence angle ϑ_s.

Inversion methods in two or three dimensions are essentially the same. In the following we consider the two dimensional case, i.e. the medium properties are not changing along the y-axis and the source is a line source along this axis.

Point source

Consider the experiment where a two dimensional medium is probed by a point source (in 2D) and the scattered field is observed all around the medium. Let $P_e(\underline{r},\omega)$ be the wavefield extrapolated from the receivers back into the medium. In the time domain, the extrapolated field can be obtained by running the homogeneous wave equation "backwards" in time with boundary conditions given by the time-reversed scattered field. It can be shown (Esmersoy et. al., 1985) that within the Born approximation the extrapolated field can be expressed as

$$P_e^*(\underline{r},\omega) = k^2 \int_V d\underline{r}'\ \gamma(\underline{r}')\ G_0(\underline{r}',\underline{r}_s)\ 2i\,\mathrm{Im}[\ G_0(\underline{r},\underline{r}')\ ]\ . \tag{2}$$

Here, G_0 is the Green's function, $\underline{r}_s$ is the source location and we have assumed an impulse source. Note that the imaginary part of the Green's function is odd symmetric in time. The causal part represents the waves converging towards the scatterers and the anti-causal part represents the outgoing waves that have passed the focus. Now, consider the following quantity obtained by imaging the filtered extrapolated field at time zero,

$$\hat{\gamma}(\underline{r}) = -4|\underline{r}-\underline{r}_s| \int_{-\infty}^{\infty} d\omega\ \frac{P_e(\underline{r},\omega)}{|\omega|}\ . \tag{3}$$

It was shown by Esmersoy et. al., 1985, that this zero time image field gives the projections of the velocity function. More specifically,

$$\hat{\gamma}(\vartheta,r) = \int_{(\underline{r}'-\underline{r}_s)\cdot\underline{u}_\vartheta=\frac{r}{2}} dl\ \gamma(\underline{r}')\ , \tag{4}$$

where (ϑ,r) are the polar coordinates centered at the source and $\underline{u}_\vartheta$ is the unit vector corresponding to the angle ϑ. Recovering $\gamma(\underline{r})$ from its projections is exactly the problem encountered in tomography and is accomplished by the inverse Radon transform.

Figure 1 shows the contour plot of the velocity structure used for the following example. Solid and dotted contours represent high and low velocities with respect to the background (750 m/s) with contour level increments of 10 m/s. The difference between the peak velocities is about 14% of the background velocity and the distance between the peaks is about one dominant wavelength. The synthetic data is obtained with a finite difference algorithm. A 50 Hz cut-off frequency Blackman-Harris window is

used as the source wavelet. Inversion is done as follows

1) According to equation (3) the observed traces are Hilbert transformed and integrated.

2) The resulting traces are extrapolated with a finite difference scheme and imaged at time zero. The zero-time image field is shown in figure 2a. This zero-time image is then weighted by the radial distance from the source. The projections are obtained from the image by picking up points along the radial lines passing through the source point. This is shown in figure 2b.

3) The velocity function is then reconstructed from its projections by the inverse Radon transform. Figures 3a and 3b show the true and the inverted velocities respectively, with identical contour levels.

Plane wave source

Consider the experiment shown in figure 4. A two dimensional medium is probed by a wide-band plane wave with incidence angle ϑ_s and the scattered field is observed along the x-axis. Note that the x-axis represents the surface for surface data and it corresponds to a vertical array in VSP. The plane wave source can be obtained by an array of point sources or it may represent the far field of a single point source. For this experiment, the volume integral of the scattered field within the homogeneous Born approximation is given by

$$P_s(x_R,\omega) = \frac{\omega^2}{c^2} \int_V d\underline{r}'\, \gamma(\underline{r}')\, e^{i\frac{\omega}{c}\hat{\underline{k}}_s \cdot \underline{r}'}\, \frac{i}{4} H_0^{(1)}\left(\frac{\omega}{c}|\underline{r}_R - \underline{r}'|\right), \qquad (5)$$

where $\underline{r}_R = (x_R,0)$ is the receiver coordinate, $\hat{\underline{k}}_s$ is the unit vector along the incident direction of the probing wave and $H_0^{(1)}$ is the Hankel function of the first kind. By taking the spatial Fourier transform of both sides with respect to the receiver offset x_R we obtain the following relation between the velocity function and the observed scattered field,

$$\tilde{\gamma}\left[\frac{\omega}{c}\left(\hat{\underline{k}} - \hat{\underline{k}}_s\right)\right] = \frac{2\sin\vartheta}{ik}\, \tilde{P}_s\left(\omega\frac{\cos\vartheta}{c},\omega\right). \qquad (6)$$

Here, ϑ is the polar angle in the Fourier domain, $\hat{\underline{k}}$ is the unit vector cooresponding to this angle and $k_x = (\omega/c)\cos\vartheta$ is the horizontal wavenumber. Now, for fixed ϑ, the $\tilde{P}_s$ term on the right hand side is simply the Fourier transform of the slant-stacked data taken with respect to the intercept variable τ for a fixed slope $p = \cos\vartheta/c$. Polar

coordinates of the argument of $\tilde{\gamma}$ are given by

$$\Omega \equiv \frac{\omega}{c} \mid \hat{\underline{k}} - \hat{\underline{k}}_s \mid = \omega \frac{2}{c} \sin(\frac{\vartheta - \vartheta_s}{2}) \tag{7a}$$

$$\varphi \equiv \text{angle} (\hat{\underline{k}} - \hat{\underline{k}}_s) = \frac{1}{2} (\vartheta + \vartheta_s - \pi) . \tag{7b}$$

Thus, for fixed ϑ, the argument of $\tilde{\gamma}$ is a radial line with polar angle φ. Finally, due to the projection-slice theorem, the projection of the velocity function $\gamma(\underline{r})$ with projection angle φ is obtained by filtering the slant-stack with slope $p = \cos\vartheta / c$ over the intercept variable and strecthing according to equation (7a) as shown in figure 5. For a single line array only the portion of the scattered field that propagate towards the receivers is observed, therefore, we have the constraint that $-\pi < \vartheta < 0$. This means that, for a given plane wave with incidence angle ϑ_s, $\tilde{\gamma}$ can be recovered in the shaded region shown in figure 6. It is easy to conclude that, for complete coverage either two plane waves incident from opposite directions or two line arrays on both sides of the scatterer are sufficient.

The velocity function can be reconstructed from the observed traces as follows. From Radon's inversion formula (Dudgeon and Mersereau, 1984)

$$\gamma(\underline{r}) = \frac{1}{4\pi^2} \int_{\Phi} d\varphi \int_{-\infty}^{\infty} d\Omega \, |\Omega| \, \tilde{\gamma}(\varphi,\Omega) \, e^{i\Omega \underline{u}_\varphi \cdot \underline{r}} , \tag{8}$$

where $\underline{u}_\varphi$ is the unit vector associated with the angle φ and Φ is the range of available projections. By changing variables from (φ,Ω) to (ϑ,ω) the final result is given by

$$\gamma(\underline{r}) = \frac{1}{\pi} \int_0^{\pi} d\vartheta \, \sin\vartheta \, \sin^2(\frac{\vartheta - \vartheta_s}{2}) \, Q(\vartheta,\underline{r}) , \tag{9}$$

where

$$Q(\vartheta,\underline{r}) = -\frac{1}{2} \int_{-\infty}^{\infty} d\omega \, i sgn(\omega) \, \tilde{P}_s(\omega \frac{\cos\vartheta}{c},\omega) \, e^{i\omega \frac{2}{c} \sin(\vartheta - \vartheta_s/2)(\hat{\underline{k}} - \hat{\underline{k}}_s) \cdot \underline{r}} . \tag{10}$$

In summary, medium velocities are obtained by the following sequence of operations :

1) Slant-stack the observed data and hilbert transform over the intercept variable τ.

2) For each slope p stretch the τ axis according to equation (10). This gives the filtered projections.

3) Backproject and weight each projection as shown in equation (9).

Acknowledgements

The work of B. C. Levy was supported in part by the Army Research Office under Grant No. DAAG29-84-K-0005.

References

Clayton, R. W. and Stolt, R. H.,"A Born-WKBJ inversion method for acoustic reflection data," Geophysics, Vol. 46, No. 11, November 1981.

Cohen, J. K. and Bleistein, N.,"Velocity inversion procedure for acoustic waves," Geophysics, Vol. 44, No. 6, June 1979.

Devaney, A. J.,"Geophysical Diffraction Tomography," IEEE Trans. Geosience and Remote Sensing, Vol. GE-22, No. 1, January 1984.

Dudgeon, D. E. and Mersereau, R. M., Multidimensional digital signal processing, Prentice-Hall, Inc., New Jersey, 1984.

Esmersoy, C., Oristaglio, M. L. and Levy, B. C.,"Multidimensional Born velocity inversion: Single wide-band point source," to appear in the J. Acoust. Soc. Am.

Mueller, R. K., Kaveh, M. and Wade G.,"Reconstructive Tomography and Applications to Ultrasonics," Proc. IEEE, Vol. 67, No. 4, April 1979.

Raz, S.,"Three-dimensional velocity profile inversion from finite-offset scattering data," Geophysics, Vol. 46, No. 6, June 1981b.

Wolf, E.,"Three-dimensional structure determination of semi-transparent objects from holographic data," Optics Communications, Vol. 1, 1969.

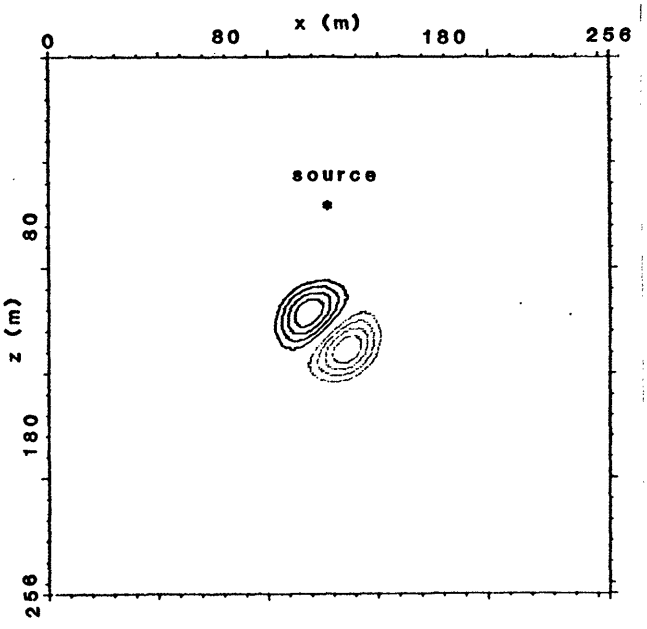

Figure 1. Velocity structure used for synthetics.

Figure 2. a) The zero-time image. b) Projections obtained from the zero-time image.

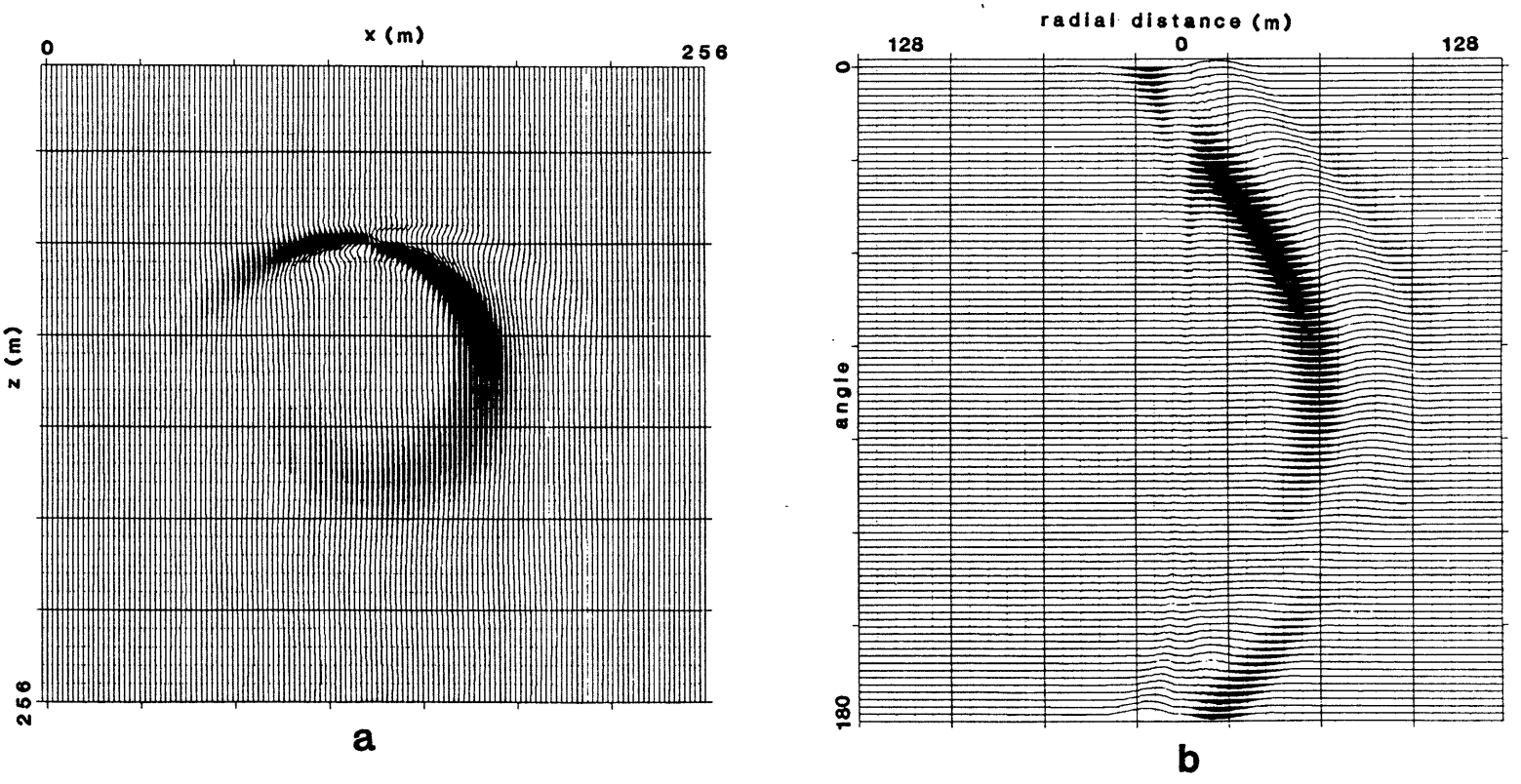

Figure 3. a) True velocity structure. b) Reconstructed velocity structure.

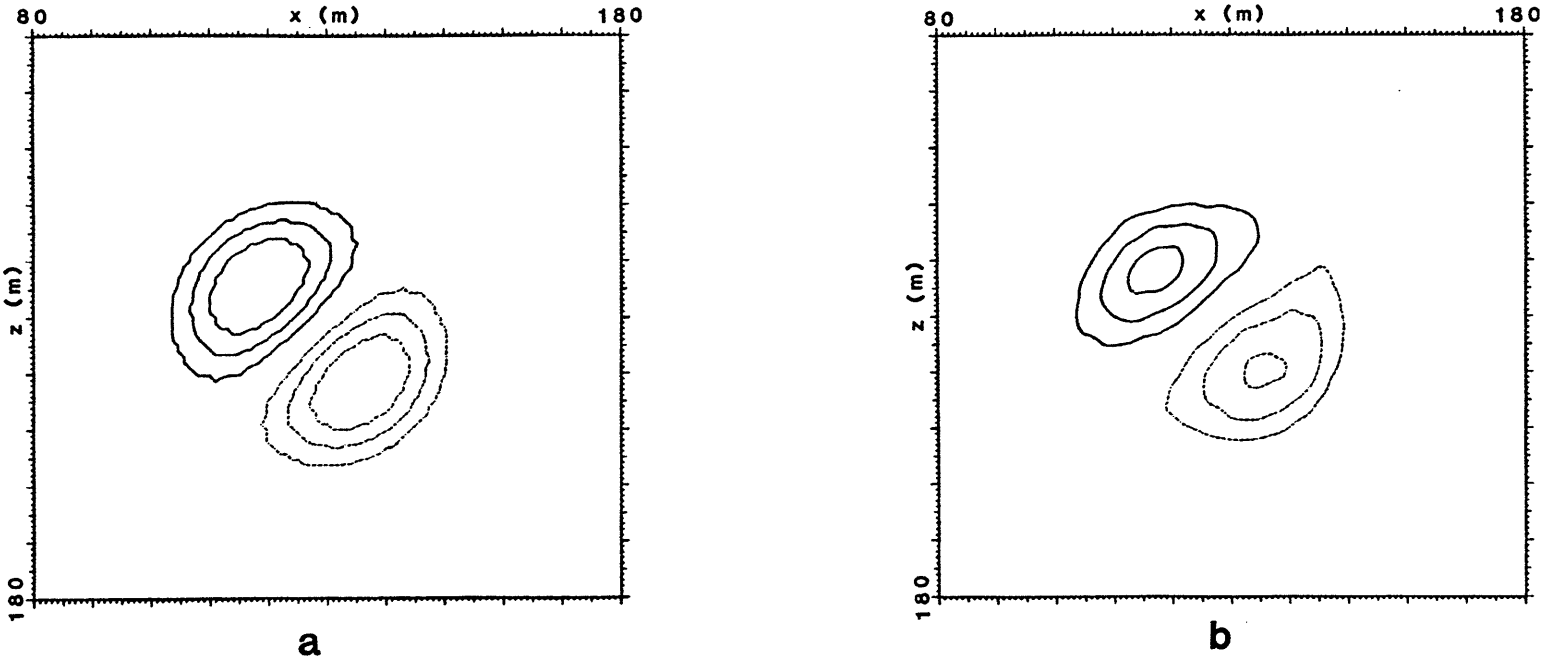

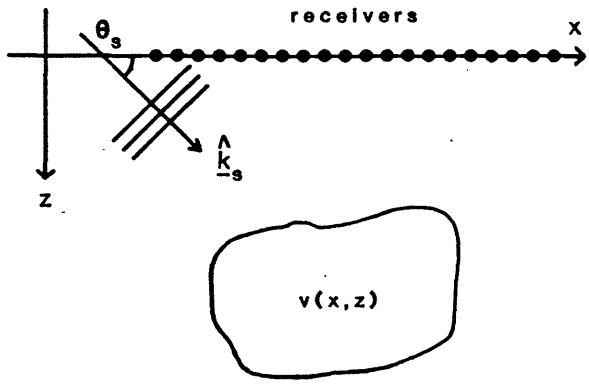

Figure 4. Plane-wave source experiment.

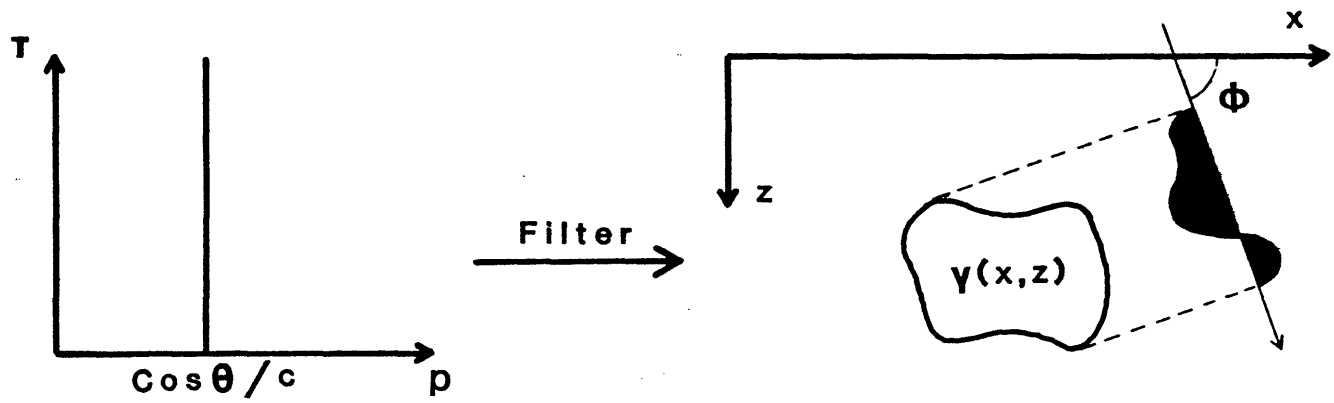

Figure 5. Projections obtained from slant-stacked data.

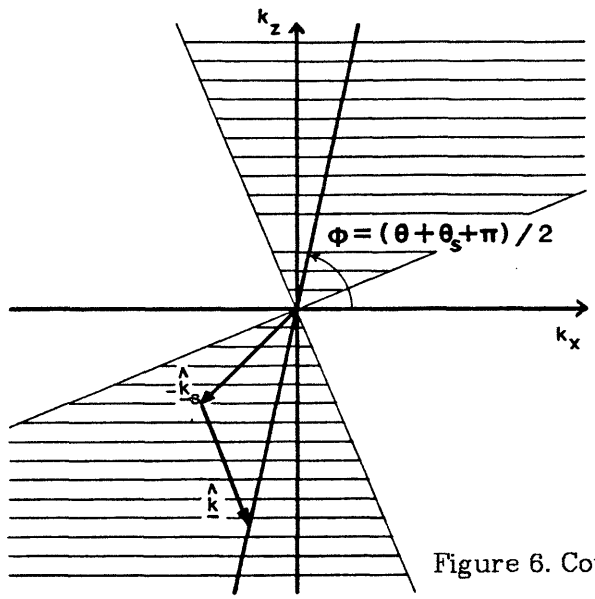

Figure 6. Coverage in the Fourier transform domain $\tilde{\gamma}(k_x,k_z)$.